Electrical characteristics of Al x Ga 1 − x N Schottky diodes prepared by a two-step surface treatment

Abhishek Motayed, Ashok Sharma, Kenneth A. Jones, Michael A. Derenge, Agis A. Iliadis, and S. Noor Mohammad

Citation: Journal of Applied Physics **96**, 3286 (2004); doi: 10.1063/1.1769096
View online: http://dx.doi.org/10.1063/1.1769096
View Table of Contents: http://scitation.aip.org/content/aip/journal/jap/96/6?ver=pdfcov
Published by the AIP Publishing

Electrical characteristics of $Al_xGa_{1-x}N$ Schottky diodes prepared by a two-step surface treatment

Abhishek Motayed
Electrical Engineering Department, Howard University, 2300 Sixth Street NW, Washington, D.C. 20059

Ashok Sharma
Component Technology and Radiation Branch, NASA Goddard Space Flight Center, Greenbelt, Maryland 20771

Kenneth A. Jones and Michael A. Derenge
U.S. Army Research Laboratory, Mail Stop AMSRL-SE-RL, Adelphi, Maryland 20783

Agis A. Iliadis
Department of Electrical & Computer Engineering, University of Maryland, College Park, Maryland 20742

S. Noor Mohammad[a)]
Electrical Engineering Department, Howard University, 2300 Sixth Street NW, Washington, District of Columbia 20059

(Received 11 July 2003; accepted 17 May 2004)

Near-ideal Schottky barrier contacts to *n*-type $Al_{0.22}Ga_{0.78}N$ have been developed by a two-step surface treatment technique. Plasma etching of the $Al_xGa_{1-x}N$ surface prior to Schottky metal deposition, combined with sequential chemical treatment of the etched surface, holds promise for developing high quality low-leakage Schottky contacts for low noise applications and for recessed gate high electron mobility transistors. In this work, the effect of postetch chemical treatment of the *n*-type $Al_{0.22}Ga_{0.78}N$ surface on the performance of the Ni/Au based Schottky contact has been investigated. Three different types of chemical treatment: viz, reactive ion etching, reactive ion etching plus dipping in hot *aqua regia*, and reactive ion etching plus dipping in hot KOH, are studied. Detailed current-voltage studies of three different surface treated diodes and a comparison with as-deposited diodes reveal significant improvement in the diode characteristics. The latter surface treatment yields Ni/Au Schottky diodes with very low reverse leakage currents, breakdown voltages greater than 44 V, and an ideality factor as low as 1.14. © *2004 American Institute of Physics*. [DOI: 10.1063/1.1769096]

I. INTRODUCTION

The last several years have witnessed rapid progress in the development of optical devices based on group III nitride semiconductors.[1] Among these semiconductors, ternary solid solutions of $Al_xGa_{1-x}N$ are currently under intense study for applications in solar-blind photodetectors, lasers, and high-power, high-frequency, high-temperature high electron-mobility transistors (HEMTs).[2] An important component of the latter are metal/semiconductor (M/S) contacts to $Al_xGa_{1-x}N$. Some studies of these contacts address the barrier heights of the Schottky contacts[3–8] to *n*-$Al_xGa_{1-x}N$; others explore the influence of the Al mole fraction on the contact barrier heights.[5,7,8] No report has appeared that touches on the reverse breakdown characteristics of the $Al_xGa_{1-x}N$ Schottky contacts.[9–14] Experimental studies of the gate current leakage in AlGaN HEMTs shows that the excess gate leakage strongly influences the gate control and the power consumption. The noise performance of the $GaN/Al_xGa_{1-x}N$ HEMTs is also dependent on the gate leakage current.[15] Thus, the reduction of the leakage current is essential for developing III-V nitride based low-noise devices. These diodes should indeed be optimized for fabrication processing for low-leakage and reliable performance. The ability to effectively modulate the M/S depletion layer width in a Schottky diode with a low reverse leakage current is the key to developing III-V nitride based low-noise electronics. Experimental studies of gate leakage current show that the excess gate leakage current strongly influences the gate control, the power consumption, and the noise performance of the $GaN/Al_xGa_{1-x}N$ based field-effect transistors.[15] It is believed that the presence of an as-deposited thin insulating layer on the $Al_xGa_{1-x}N$ surface significantly affects the current-voltage characteristics of these Schottky diodes, yet no attempts have been made so far to address this problem.

It is accepted that, due to substantial ionic components of the bonds in III-V nitrides, the Fermi level at the metal-nitride interface is unpinned.[16] This mean that nonoptimized surface preparation conditions can strongly influence the ultimate current-voltage (*I-V*) characteristics leading to non-ideal behavior of the Schottky contacts.[14,17] The impact of such effects on the $Al_xGa_{1-x}N$ Schottky diodes is not yet known. Not many studies have been conducted to determine

[a)]Author to whom correspondence should be addressed; electronic mail: snmohammad2002@yahoo.com

the plasma-induced damage of these Schottky diodes. However, from a technological viewpoint this is crucial for developing low-noise nitride based devices.

The objective of the present investigation is to carry out an in-depth investigation of the influence of the $Al_xGa_{1-x}N$ surface preparation on the current-voltage and capacitance-voltage (*C-V*) characteristics of the metal/$Al_xGa_{1-x}N$ Schottky diodes. For the investigation, attention will be focused on how to optimize the chemical treatments of the $Al_xGa_{1-x}N$ surface to improve the Schottky diode properties. The fundamentals and the microstructure of these Schottky diodes will be addressed in a subsequent investigation.

II. GROWTH AND FABRICATION

The $Al_xGa_{1-x}N$ layer for this study was grown on 400 μm thick (0001) sapphire substrates at the U.S. Army Research Laboratory by employing the metal organic chemical vapor deposition method. First, a 30 nm thick low temperature (500 °C) undoped GaN buffer layer was deposited. It was followed by the growth of a 1.4 μm thick layer of $Al_xGa_{1-x}N$ at 1070 °C with $x=0.10-0.22$. From Hall measurements the background donor concentration was found to be around 1.6×10^{16} cm^{-3}.

Four samples were cut from the same wafer and were cleaned by degreasing in a soap solution followed by 3 min heated ultrasonic baths successively in trichloroethylene, acetone, and methanol. The samples were then dipped in a heated bath of an $NH_4OH:H_2O_2:H_2O$ (1:1:5) mixture for 3 min, followed by a 3 min dip in a heated $HCl:H_2O_2:H_2O$ (1:1:5) mixture. One of the samples was removed at this stage, and no further treatment was done to it. It was labeled sample A_0. The remaining three samples were reactively ion etched (RIE) for 15 sec at 150 W in our Plasma Therm 790 System with Cl_2. The Cl_2 flow rate was 15 SCCM (SCCM denoter cubic centimeter per minute at STP), and the chamber pressure was 10 mTorr. This resulted in an etch depth of 325 Å.

The RIE etching parameters were optimized to induce as little surface damage as possible. However, plasma etching does produce some damage to the surface. The damaged surfaces are generally very prone to subsequent oxide formation, which adversely affects the contact performance,[18] so efforts were made to prevent the samples from being exposed to air for any extended period of time after they were brought out of the RIE chamber. All the samples were kept immersed in methanol during the idle time of processing. The second sample, B_0, was left as etched with no post etch treatments. The third sample, C_0, was immersed in boiling aqua regia for 5 min, while the fourth sample, called sample D_0, was immersed in boiling KOH (45%) solution for 5 min.

Schottky diodes were fabricated using two-step photolithography. The ohmic Ti/Al/Ti/Au (300 Å/1000 Å/300 Å/300 Å) contact metal evaporation was followed by a standard lift off in acetone. These contacts formed rings with an inner diameter of 300 μm and an outer diameter of 375 μm. All but the Au were electron beam evaporated, and it was evaporated thermally. The ohmic anneal was done by rapid thermal annealing at 750 °C for 30 sec in a flowing argon gas. Prior to Schottky metal deposition, the samples were dipped into $HF:HCl:H_2O$ (1:1:10) for 15 sec, and then rinsed in H_2O and blown dry. 200 μm diameter Schottky contacts were aligned inside the 300 μm opening in the ohmic contacts by evaporating 500 Å of Ni followed by 250 Å of Au. Following photolithography, but during evaporation the base pressure of the vacuum chamber was maintained at about 10^{-7} Torr, and the substrates were kept at room temperature.

Electrical characterization of all the diodes included *I-V* and *C-V* measurements. *I-V* measurements of the diodes were made at room temperature using a Sony Tektronix 370-A Curve Tracer interfaced with a computer. From the *I-V* plots forward/reverse voltage drop, reverse saturation current, and breakdown voltage were determined. *C-V* measurements were made using a computer-interfaced HP 4912-A. Impedance analyzer meter connected to a probe station in the parallel mode. The measurement frequency was fixed at 100 kHz.

III. RESULTS AND DISCUSSION

A. Current-voltage characteristics—forward bias

The *I-V* characteristics of the Ni/Au Schottky contacts made on the untreated $Al_xGa_{1-x}N$ surface and the surfaces treated by the three other different methods are shown in Figs. 1(a)–1(c). Figure 1(a) compares the *I-V* characteristics of all four diodes. Corresponding to the same applied bias, the current in the A_0 diode is on the order of 10^{-5} A, while the currents in the B_0, C_0, and D_0 diodes are on the order of 10^{-3} A. For the sake of clarity, the enlarged view of the *I-V* characteristics of the A_0 diode is shown by itself in Fig. 1(b). It can be seen that the forward conduction of the A_0 diode started at the relatively high voltage of ~4 V. The reverse breakdown voltage for this diode was slightly over 6 V, which is far below the theoretical limit.

From Fig. 1(a) one can see that significant improvement in the forward conducting voltage took place due to the surface treatment for all of the diodes. The forward conduction started at as low as 0.5 V in the RIE etched only (B_0) diodes. Yet, compared to the untreated diodes (0.5 μA at 4 V), the leakage current increased to a significant value of 0.105 mA at −4 V under reverse bias. Although the B_0 diodes had excellent forward conduction properties, they had a lower reverse breakdown voltage and a higher leakage current, which may be attributed to RIE ion-induced damaged.

Of the three diodes with surface treatments, the diodes that had undergone RIE and were subsequently boiled in aqua regia (C_0), showed the maximum degradation in both the forward conduction and reverse leakage currents. These soft breakdown characteristics observed in the A_0, B_0, and the C_0 diodes were mainly due to the interface current arising from high surface states at the M/S interface. Notably the A_0, B_0, and C_0 diodes had higher interface states than the D_0 diodes. Although we have not tested for it, the tunneling along the contact edges due to the high electric field at the contact periphery may also be a possibility for the higher leakage current.

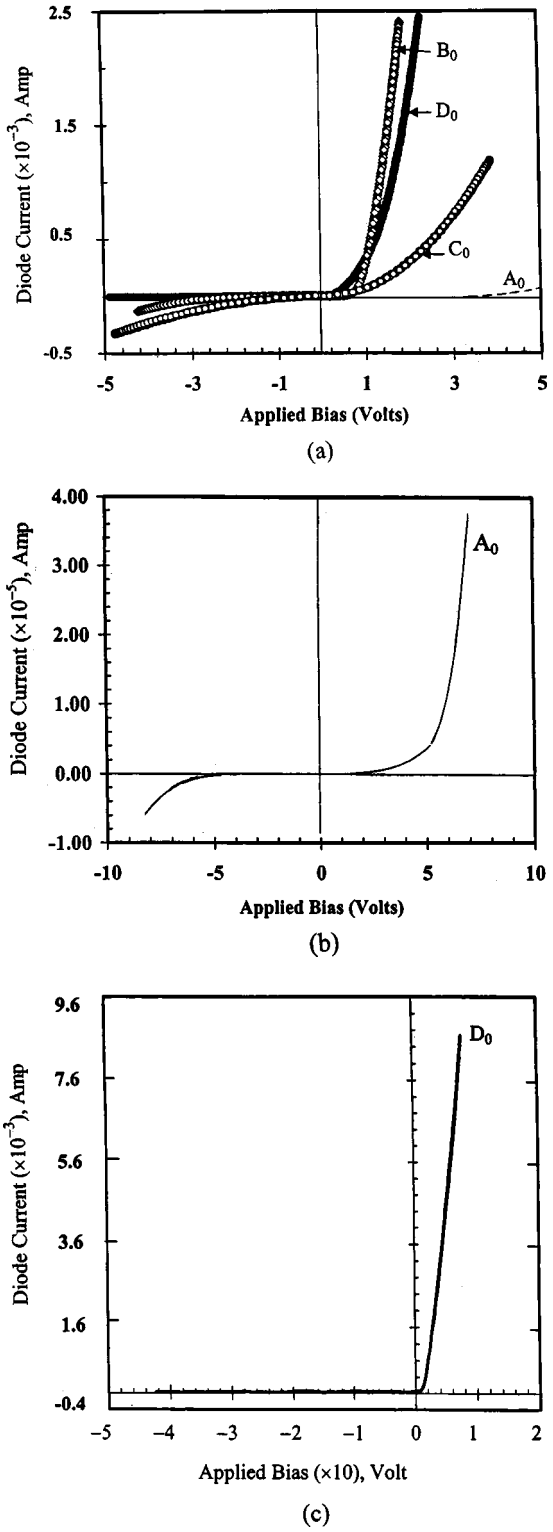

FIG. 1. (a) Absolute diode current vs voltage curves for A_0, B_0, C_0, and D_0 Au/Ni/$Al_xGa_{1-x}N$ diodes. (b) Enlarged view of the diode current vs voltage curve for the A_0 diodes. (c) The diode current vs voltage curve showing large reverse breakdown for the D_0 diodes.

The most striking feature of the present study was revealed from the *I-V* characteristics of the RIE etched diodes that were wet etched in KOH (e.g., D_0 diodes). They demonstrated a significant increase in the reverse breakdown voltage and a dramatic decrease in the leakage current. Figure 1(c) shows the full-scale *I-V* characteristics of the D_0 diodes, which exhibited a breakdown voltage of 45 V. Remarkably, this is an order of magnitude higher than that of the untreated diodes. Unlike other diodes, the D_0 diodes also had hard breakdown characteristics in that they had leakage current density on the order of 3×10^{-3} A/cm^2 at 18 V.

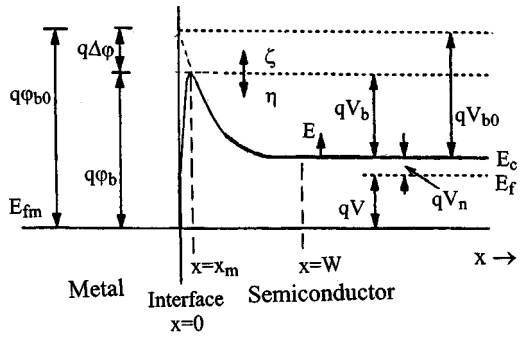

FIG. 2. Schematic diagram of the band structure of a metal-semiconductor contact under forward bias.

A schematic diagram of the band structure of the *n*-$Al_xGa_{1-x}N$ Schottky diode under forward bias[3] is shown in Fig. 2. In this figure E_f is the Fermi level of the semiconductor, E_{fm} is the Fermi level of the metal, E_c is the conduction band edge of the semiconductor, ξ is the energy of electrons above the top of the effective barrier, η is the energy of the electrons below the top of the effective barrier, E is the energy of electrons measured from E_c, V is the applied voltage, $qV_n=E_c-E_f$, $q\phi_{b0}$ is the barrier height of the contact ignoring image force lowering, and $q\Delta\phi$ is the image force lowering of the barrier height. The effective barrier height is $q\phi_{b0}-q\Delta\phi$, and the effective flat-band voltage is $qV_b=qV_{b0}-q\Delta\phi$. The Fermi level, E_f, is positive when above the bottom of the conduction band edge E_c.

Current I through a Schottky barrier junction resulting from the conventional thermionic emission may be expressed by[19]

$$I = I_0 \exp\left(\frac{qV}{n_{idl}k_BT}\right)\left[1-\exp\left(-\frac{qV}{k_BT}\right)\right], \tag{1}$$

where I_0 is the reverse saturation current given by

$$I_0 = AA^{*}T^2 \exp\left(-\frac{q\varphi_B}{k_BT}\right), \tag{2}$$

where A is the surface area of the metal-semiconductor interface (area of the diode), A^* is the Richardson constant, q is the electronic charge, T is the absolute temperature of the metal-semiconductor junction, φ_B is the Schottky barrier height of the metal-semiconductor junction, k_B is the Boltzmann constant, V is the applied voltage, and n_{idl} is the ideality factor. Carrier transport across the M/S interface of ideal diodes occurs strictly via thermionic emission, and for ideal diodes the ideality factor n_{idl} included in Eq. (1) is unity. Equation (1) can be manipulated to the form[19]

$$\mathrm{In}(\xi_{VN}) = m_{VN}V + c_{VN}, \tag{3}$$

where

$$\xi_{VN} = \left[I\left\{1-\exp\left(-\frac{qV}{k_BT}\right)\right\}^{-1}\right], \tag{4}$$

$$m_{VN} = \left(\frac{q}{n_{idl} k_B T} \right), \tag{5}$$

$$c_{VN} = \ln(I_0). \tag{6}$$

This means that, experimentally, the ideality factor n_{idl} of a diode can be extracted from a logarithmic plot of ξ_{VN} as a function of the applied bias V. Experimentally observed I-V characteristics of diodes differ frequently from the theoretical predictions made on the basis of thermionic emission theory. A departure from the ideality is caused by the image force lowering, generation and recombination of carriers in the space charge region, interface states, and thermionic field emission.[20–23] These effects invariably increase the ideality factor. Hence the factor is indicative of how close to ideality the Schottky diode is.

The drift and diffusion of carriers may also play a role in the carrier transport through the M/S contact. It can be described in terms of an effective diffusion velocity. v_D, associated with the transport of electrons from the edge of the depletion region, $x=W$ (see Fig. 2) to the point ($x=x_m$) where the potential energy is maximum. However, these phenomena become effective if the barrier height is much larger than the thermal voltage, k_BT, the effect of electron collisions within the depletion region is appreciable, the carrier concentrations at the edge of the depletion region is unaffected by the current flow (e.g., they have the equilibrium value), and the ionized impurity concentration in the semiconductor is low. The diffusion of carriers is strongly influenced by the potential configuration of the region through which the diffusion occurs. This potential configuration at the M/S interface ($x=0$) is affected by image force lowering. Because of this, there occurs a rounding of the potential energy $q\psi(x)$ near the M/S interface, and the potential energy becomes lower at the M/S interface ($x=0$) than at $x=x_m$. The portion of the barrier between $x=0$ and $x=x_m$ thus acts as a sink for electrons. Under these circumstances the current flow across the junction is better described in terms of an effective recombination velocity, V_R, at the potential energy maximum at $x=x_m$. If $V_D \ll V_R$ the drift-diffusion process is very dominant. On the other hand, if $V_D \gg V_R$ the thermionic process is dominant.[24]

Figure 3 shows the logarithmic plot of the forward current density for all four diodes. One can see that there is a major improvement in the forward current density due to RIE etching of the surface prior to metal deposition. We attribute it to the removal of the native oxide present on the surface of the virgin samples. Formation of such a native oxide impedes the current conduction until the electric field sustained by the thin interfacial layer is strong enough for the carriers to tunnel through it. This is manifested by a higher forward conduction voltage observed in the untreated sample diodes.

From Fig. 3 it can be seen that there was a decrease in series resistance in the B_0 diodes as compared to the A_0 diodes. Previous investigations of the effects of surface treatments of the GaN surface have also shown that removal of native oxides improve the contact resistance.[25] This is expected because, in n-GaN, the dry etch damage leads to higher near-surface conductivity.[26] It is apparent that the series resistance of the D_0 diodes was larger than that of the B_0 diodes. The dry-etching damage extended up to a few 100 Å, and it was removed by the subsequent boiling in hot KOH for 5 min. The immediate result was that the removal of the damaged n-type conducting layer accompanied an increase in the series resistance of the D_0 diodes. The forward current density for the C_0 diodes differ markedly from those of the other diodes that had received surface treatments. We will later show that the reverse current density and the plots for the ideality factor, n_{idl}, indicated that the RIE-etching damage was not, in fact, fully removed using the aqua regia treatment.

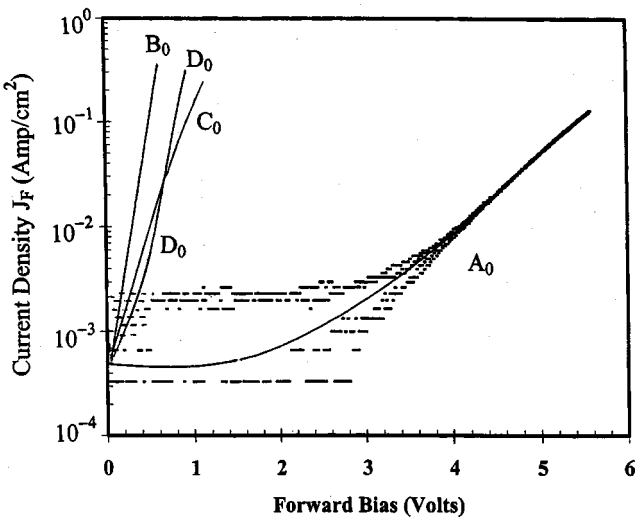

FIG. 3. Semilogarithmic plot of forward current density vs forward applied bias for A_0, B_0, C_0, and D_0 diodes.

The ideality factor for the diodes was obtained from the $\ln(\xi_{VN})$ vs V plots, which are shown in Figs. 4(a) and 4(b). As indicated earlier, our measurement tools have low precision for measurements of low current. So spurious data points in the form of small plus signs, multiple signs and circles appear in these figures. The ideality factor n_{idl} is extracted from the straight line portion of each of the plots, and are listed in Table I. The ideality factor for the untreated diodes was quite high suggesting that the transport in this diode involved complex processes including tunneling through insulating layers. The ideality factor extracted for the RIE only treated diodes was as high as 13.5 plausibly because the tunneling mediated current transport mechanism was very dominant for these diodes. In contrast, the aqua regia treated diodes had a lower ideality factor of 6.8. For the KOH treated diodes, the ideality factor was as low as 1.14, which is close to that of an ideal diode.

B. Current-voltage characteristics-reverse bias

The leakage current observed experimentally in our diodes can be analyzed at least qualitatively by taking into consideration various transport mechanisms such as tunneling through the Schottky barrier, generation and recombination in the depletion layer, and defect assisted conduction in various diodes making use of the inhomogeneously "patchy" Schottky barrier model.[27] The total reverse current density,

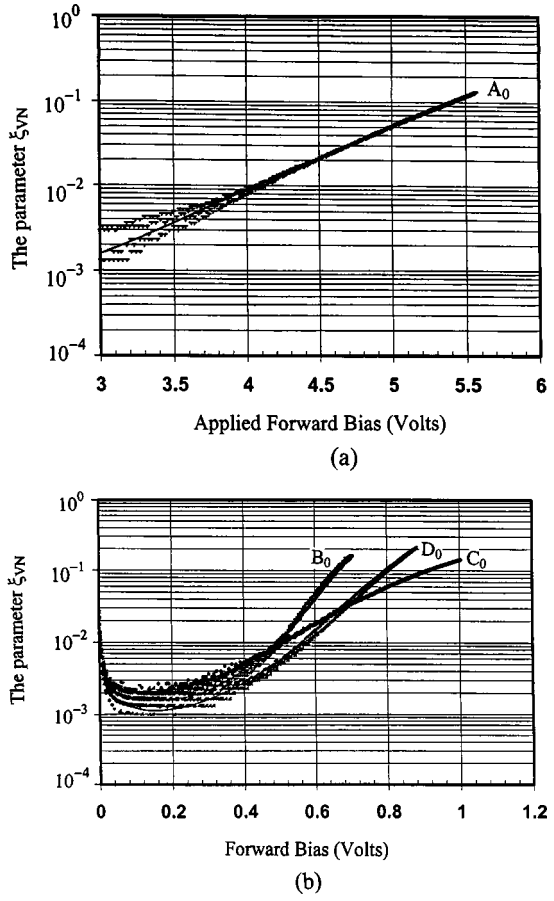

FIG. 4. Semilogarithmic plots of ξ_{VN} as a function of the applied bias for (a) the A_0 diodes and (b) the three surface treated B_0, C_0, and D_0 diodes.

J_{REV}, through the Schottky barrier can be assumed to be the sum of current density components arising from various electrical mechanisms:

$$J_{\mathrm{REV}} = J_{\mathrm{TE}} + J_{\mathrm{TUN}} + J_{\mathrm{GR}} + J_{\mathrm{MS}}. \tag{7}$$

J_{TE} is the thermionic emission current density. J_{TUN} is the tunneling current component density, which dominates in degenerate semiconductors at low temperatures. J_{GR} is the generation-recombination current density arising mainly in the depletion region. J_{MS} the thermionic field emission current density in the presence of traps defects at the metal-semiconductor interface.

According to the thermionic emission theory, the reverse current density is given by the same equations as those for forward bias, but they are applied to the region where V is negative. Except at high temperatures and voltages, the reverse thermionic emission current density is negligibly small. The tunneling component of the leakage current density may be given by[3]

$$J_{\mathrm{TUN}} = \frac{A^* T}{k_B}\int_0^{qV_b} \exp\left(-\frac{qV_b - qV}{k_B T}\right) \times \exp\left(\frac{\zeta}{k_B T}\right)\exp\left(-\frac{\zeta}{E_0}\right)d\zeta \tag{8}$$

$$= \frac{A^* T^2}{\alpha_0}\left[\exp\left(\frac{qV - q\varphi_b}{k_B T}\right) - \exp\left(\frac{qV - q\varphi_b}{E_0}\right)\exp\left(\frac{q\alpha_0 V_n}{k_B T}\right)\right], \tag{9}$$

where

$$E_0 = \left(\frac{8}{3q\hbar}\sqrt{\frac{m_n^* \varepsilon_0 \varepsilon_s}{N_d}}\right)^{-1}, \tag{10}$$

$$qV_b = q\varphi_B - qV_n - qV, \tag{11}$$

$$\alpha_0 = \frac{k_B T}{E_0} - 1, \tag{12}$$

$\hbar = h/2\pi$, m_n^* is the effective electron mass in the conduction band, and $qV_n = E_c - E_f$.

At low applied bias, the most dominant electrical conduction is via tunneling. This is evident from the soft breakdown characteristics observed in the A_0, B_0, and C_0 diodes, but not in the D_0 diodes. The presence of defects near the surface region can give rise to defect assisted tunneling, which can greatly enhance the tunneling probability. It often is manifested by soft breakdown characteristics that are observed in all but our D_0 diodes.

For most compound semiconductors that exhibit small effective electron masses, in general, the thermionic field emission is an important component of the reverse current density. Under reverse bias, the field emission occurring from the metal into the semiconductor of the diodes can reasonably be approximated by considering a triangular barrier. Under these assumptions the reverse bias voltage is larger than a few $(k_B T/q)$ so at low temperature operation the current density due to field emission is given by the complex equation[28]

TABLE I. Summary of electrical characteristics of the four different diodes.

Sample	Treatment	Reverse breakdown voltage V_{RB} (V)	Breakdown characteristics	Forward conduction voltage V_{ON} (V)	Ideality factor	Barrier height $\varphi_B^{C\text{-}V}$ (eV)
A	Untreated	6	Soft breakdown	4.0	22.00	0.55
B	RIE etched	4	Soft breakdown	0.5	12.00	0.22
C	RIE etching+aqua regia boil	4	Soft breakdown	0.4	6.81	⋯
D	RIE etching+KOH boil	45	Hard breakdown	0.5	1.14	0.85

$$J_{\mathrm{MS}} = A^{*}\frac{E_{00}^{2}}{K_B^{2}}[1 - B_1\varphi_B^{-1}]\exp\left(-\frac{(2q\varphi_B)^{3/2}}{3E_{00}\sqrt{(q\varphi_B + qB_2)}}\right), \tag{13}$$

where

$$E_{00} = \frac{qh}{4\pi}\sqrt{\frac{N_d}{m_n^{*}\varepsilon_0\varepsilon_s}}, \tag{14}$$

$$B_1 = V - V_n, \tag{15}$$

$$B_2 = V + V_n. \tag{16}$$

From Eqs. (13)–(16) it is clear that a small change in the barrier height results in a significant change in the reverse thermionic field emission current density.

The threading dislocations present in the nitride materials are believed to be nonradiative recombination centers, and they can act as traps for carriers. Generation of carriers can also arise from mechanisms such as thermal electron-hole (*e*-*h*) pair generation, which is usually negligible for wide band gap semiconductors. (Under room temperature operations, so they can safely be neglected.) Other mechanisms of generation might be emission from the traps and the generation of carriers due to impact ionization. Such carriers mught be important in the presence of the high electric fields generated in reverse biased junctions. The generation-recombination current can be expressed as

$$J_{\mathrm{GR}} = \frac{qW}{2}v_{th}\sigma_T N_T n_i \exp\left(\frac{qV}{2k_BT}\right), \tag{17}$$

where W is the space charge layer (depletion layer) width, v_{th} is the saturation velocity of electrons, σ_T is the capture cross section for electrons by the traps concerned, and n_i is the intrinsic carrier concentration.

To understand the importance of the various components of the reverse leakage current, we carried out numerical calculations of J_{TE}, J_{TUN}, J_{MS}, and J_{GR}. The parameters used for the calculations are $A^{*}=26$ A cm^{-2} K^{-2}, $\varphi_B=0.85$ and 0.57 V, $N_T=1.5\times10^{9}$ cm^{-2}, $\varepsilon_s=9.10$, $m_n^{*}=0.2$, and $v_{th}\sigma_T=10^{-7}$ cm^{3} sec^{-1}. The intrinsic carrier concentration is calculated using the conventional formula. The effective density of states for electrons and holes, N_{c} and N_v, respectively, are estimated from those of GaN using Vegard's law. Thus we got $N_{\mathrm{c}}=3\times10^{18}$ cm^{-3} and $N_{\mathrm{v}}=2\times10^{19}$ cm^{-3}. The energy bandgap for $Al_xGa_{1-x}N$ was given by[1]

$$E_g^{\mathrm{AlGaN}} = (1-x)E_g^{\mathrm{GaN}} + xE_g^{\mathrm{AlN}} - bx(1-x), \tag{18}$$

where $E_g^{\mathrm{GaN}}=3.39$ eV, $E_g^{\mathrm{AlN}}=6.20$ eV, and b is the bowing parameter with a value of 0.96. Various current densities were computed for a number of different ideality factors ranging between 1.0 and 10.0. These results for certain representative n_{idl} values are listed in Table II. In this table, for each applied bias, the first, second, third, and fourth data of column 2 correspond to $n_{idl}=1.0$, 4.0, 7.0, and 10.0, respectively; the first, second, third, and fourth data of column 3, however, correspond to $n_{idl}=1.0, 1.1, 1.2$, and 1.3, respectively. The experimental data for C_0 and D_0 diodes are presented in columns 4 and 5 of the table. It was observed that, for $n_{idl}=1.0$, the calculated current density for the thermionic emission, tunneling, and the thermionic field emission are negligibly small—lower than about 10^{-10} A/cm^2. However, for larger values of n_{idl} they could not always be ignored. This is because n_{idl} of J_{TE} with values greater than one for any diode represented a measure of the deviation of the diode characteristics from the ideal transport mechanisim limit, which is the thermionic emission of carriers over the barrier. Image force lowering, generation-recombination in the space charge region, interface states, and thermionic field emission should all have contributions to the possible transport mechanism, which lead the ideality factor to be greater than unity.[20–23] Thus, the contributions of all these current density components were actually lumped into the J_{TE} term with nothing left to be inferred from separate calculations for J_{TUN} and J_{MS}. Interestingly, the experimental results for C_0 diodes are close to the calculated ones for $\varphi_{\mathrm{B}}=0.57$ V and $n_{idl}=1.2$. The experimental results for C_0 diodes are essentially identical to the calculated ones for $\varphi_B=0.57$ V and $n_{idl}=1.0$. Thus confirms that the thermionic emission is the primary mechanism for reverse current in D_0 diodes; but tunneling, thermionic field emission, recombination, etc. contribute to the reverse current in C_0 diodes.

TABLE II. The C^{-2} vs V_R relationships for sample A_0, B_0, C_0, and D_0 diodes.

Diode	Relationship
Sample A_0 diode	$C^{-2}=-4.0\times10^{14}\ V_R+2.0\times10^{14}$
Sample B_0 diode	$C^{-2}=-1.846\times10^{14}\ V_R-4.307\times10^{13}$
Sample C_0 diode	$C^{-2}=-4.0\times10^{14}\ V_R+1.0\times10^{15}$
Sample D_0 diode	$C^{-2}=-9.0\times10^{14}\ V_R+6.0\times10^{14}$

Figure 5(a) shows the reverse current density plots as a function of reverse bias for the A_0, B_0, and C_0 diodes, and Fig. 5(b) shows the same plot for the D_0 diodes. Unfortunately our measurement tools do not exhibit high precision for the measurements of current density below 10^{-2} A/cm^2 so spurious data points in the form of small dashes appear in Fig. 5(a) for current densities below 10^{-2} A/cm^2. The same spurious data points appeared in the form of small crosses in Fig. 4(a), and in the form of small squares in Fig. 4(b). The reverse leakage current density for all four diodes reveal distinctive features of all three surface treatments in terms of dry-etch damage and their restoration by the subsequent chemical treatment. The RIE only surface etched diodes exhibited a higher reverse leakage current and a lower reverse breakdown voltage than the untreated diodes. This is consistent with findings by other researchers.[29,30] While the plasma etching removed the interfacial oxide and hydroxide layers, it created a shallow damaged layer due to ion bombardment. This damage consists mainly of point defects, with shallow energy levels.[29] The presence of a thin damaged interfacial layer with increased *n*-type conductivity enhanced the tunneling probability thus increasing the reverse bias leakage current. Unfortunately, the postetch treatment in boiling aqua regia did not prove to be useful in removing the plasma induced damage. As evident from Fig. 5(a), the leakage current in C_0 diodes increased more than in the B_0 diodes. Fig-

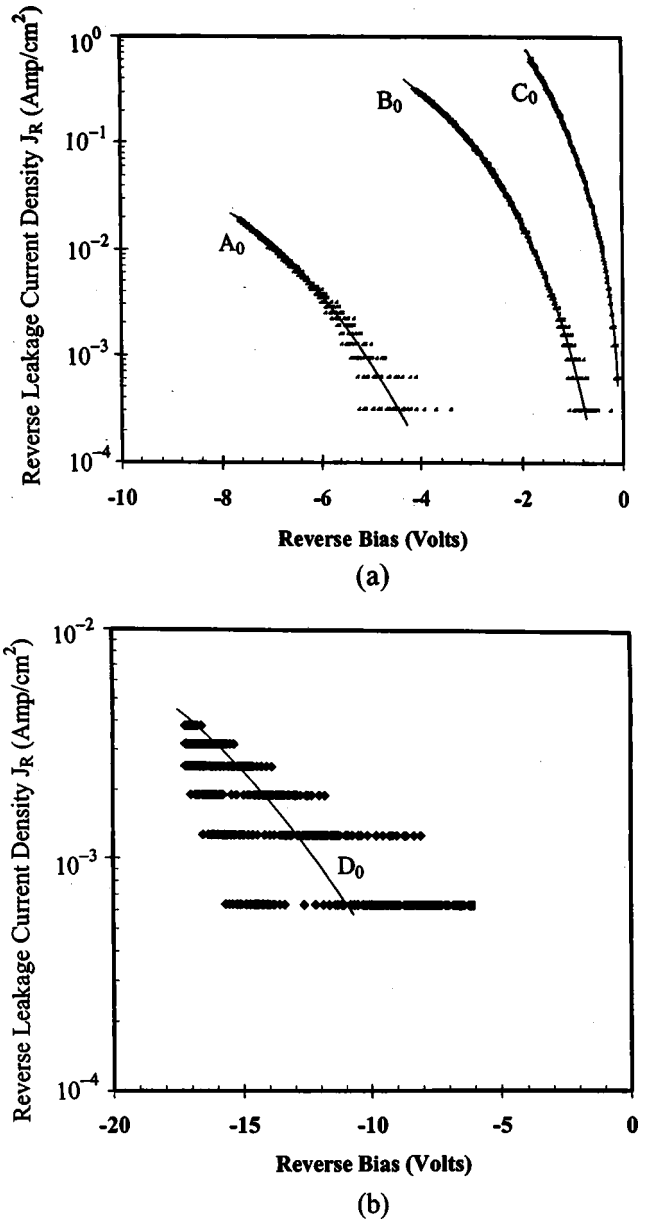

FIG. 5. (a) Semilogarithmic plot of reverse current density with respect to reverse bias for the A_0, B_0, and C_0 diodes. (b) Semilogarithmic plot of reverse current density vs reverse bias for the D_0 diodes.

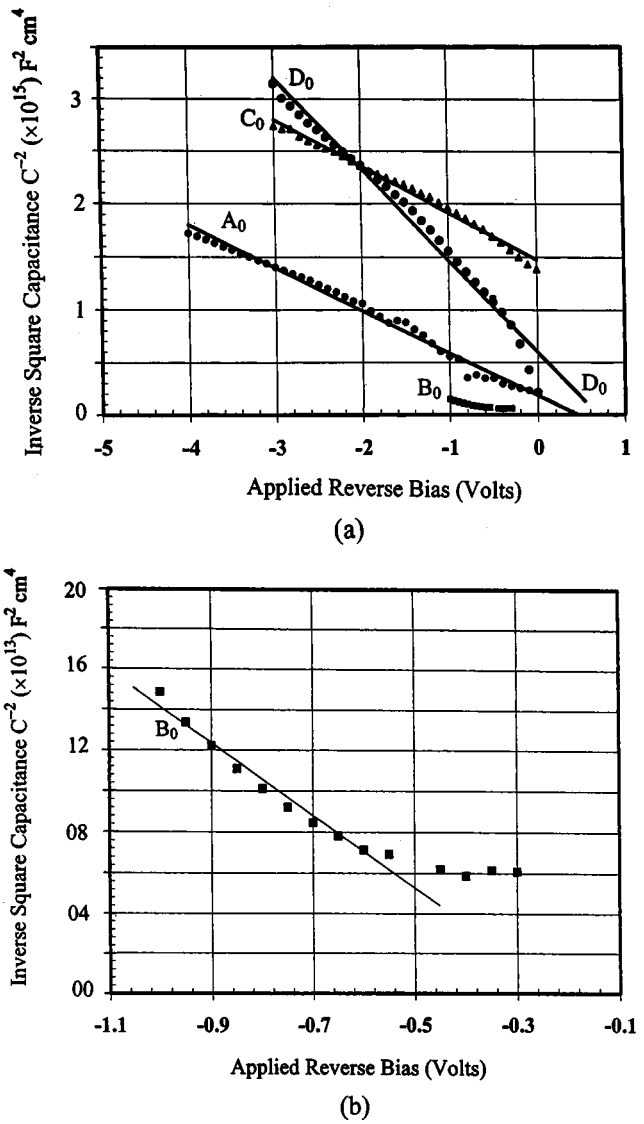

FIG. 6. (a) C^{-2} vs V plot for all four different diodes, and (b) enlarged view of the C^{-2} vs V plot for the RIE treated only B_0 diodes.

ure 5(b) reveals that indeed subsequent KOH treatment after RIE etching was very effective in minimizing the plasma-induced damage. In these diodes there was a very low level of leakage current even at high reverse voltages (e.g., 3×10^{-3} A/cm^2 at 18 V). The breakdown voltage also improved from 4 V for the B_0 diodes to over 44 V for the D_0 diodes. The results were also superior to those for the A_0 diodes.

C. Capacitance-voltage characteristics

The primary objective of the *C-V* measurements was to uncover the nature of the depletion region in the Schottky diodes. For a negligibly small thickness of the oxide layer between the metal and the uniformly doped semiconductor, the inverse square of the capacitance of a defect free diode, as a function of applied reverse bias, is given by[19]

$$C^{-2} = a_T - b_T V, \tag{19}$$

where a_T and b_T are constants defined by

$$a_T = \frac{2(qV_{bi} - k_B T)}{q^2 \varepsilon_0 \varepsilon_s N_d}, \tag{20}$$

$$b_T = \frac{2}{q\varepsilon_0 \varepsilon_s N_d}, \tag{21}$$

and where ε_0 is the permittivity in vacuum, ε_s is the dielectric constant of the $Al_xGa_{1-x}N$ semiconductor, and N_d is the doping concentration of the $Al_xGa_{1-x}N$ samples. V_{bi} is the built-in potential given by

$$V_{bi} = \varphi_B - V_n \tag{22}$$

with

TABLE III. Calculated reverse leakage current due to thermionic emission for various values of the ideality factors. In column 2, the first, second, third, and fourth data correspond to $n_{idl}=1.0, 4.0, 7.0$, and 10.0, respectively. In column 3, the first, second, third, and fourth data correspond to $n_{idl}=1.0, 1.1, 1.2$, and 1.3, respectively. The experimental data for C_0 and D_0 diodes are presented in column 4 and 5. Total reverse current density ($\mathrm{Amp/cm^2}$).

Bias (V)	$\phi_B=0.85$ V	$\phi_B=0.57$ V	C_0 diode	D_0 diode
−0.1	-1.203×10^{-8}	-6.2136×10^{-4}	-1.1000×10^{-3}	-6.366×10^{-4}
	-2.189×10^{-7}	-8.6476×10^{-4}	⋯	⋯
	-3.313×10^{-7}	-1.1592×10^{-3}	⋯	⋯
	-3.910×10^{-7}	-1.4855×10^{-3}	⋯	⋯
−0.2	-1.228×10^{-8}	-6.2136×10^{-4}	-2.3312×10^{-3}	-6.366×10^{-4}
	-4.066×10^{-6}	-1.2549×10^{-3}	⋯	⋯
	-9.315×10^{-6}	-2.2550×10^{-3}	⋯	⋯
	-1.298×10^{-5}	-3.7028×10^{-3}	⋯	⋯
−0.3	-1.229×10^{-8}	-6.2136×10^{-4}	-3.1052×10^{-3}	-6.366×10^{-4}
	-7.402×10^{-5}	-1.7845×10^{-3}	⋯	⋯
	-2.566×10^{-4}	-4.2986×10^{-3}	⋯	⋯
	-4.220×10^{-4}	-9.0448×10^{-3}	⋯	⋯
−0.4	-1.229×10^{-8}	-6.2136×10^{-4}	-4.3332×10^{-3}	-6.366×10^{-4}
	-1.346×10^{-3}	-2.5365×10^{-3}	⋯	⋯
	-7.068×10^{-3}	-8.1908×10^{-3}	⋯	⋯
	-1.372×10^{-2}	-2.2085×10^{-2}	⋯	⋯
−0.5	-1.229×10^{-8}	-6.2136×10^{-4}	-8.6712×10^{-3}	-6.366×10^{-4}
	-2.451×10^{-2}	-3.6055×10^{-3}	⋯	⋯
	-1.947×10^{-1}	-1.5609×10^{-2}	⋯	⋯
	-1.460×10^{-1}	-5.3924×10^{-2}	⋯	⋯
−0.6	-1.229×10^{-8}	-6.2136×10^{-4}	-1.7755×10^{-2}	-6.366×10^{-4}
	-4.460×10^{-1}	-5.1250×10^{-3}	⋯	⋯
	-5.361×10^{-0}	-2.9739×10^{-2}	⋯	⋯
	$-1.450\times10^{+1}$	-1.3166×10^{-1}	⋯	⋯
−0.7	-1.229×10^{-8}	-6.2136×10^{-4}	-3.3256×10^{-2}	-6.366×10^{-4}
	-8.115×10^{-0}	-7.2848×10^{-3}	⋯	⋯
	$-1.477\times10^{+2}$	-5.6665×10^{-2}	⋯	⋯
	$-4.713\times10^{+2}$	-3.2148×10^{-1}	⋯	⋯

$$V_n = \frac{k_B T}{q}\ln\left(\frac{N_c}{N_d}\right), \tag{23}$$

where N_c is the effective density of states for electrons in the conduction band.

The room-temperature variation of C^{-2} (per $\mathrm{cm^2}$) with the applied reverse bias at a frequency of 100 KHz is shown in Figs. 6(a) and 6(b) for all four diodes. Figure 6(b) shows the same plot for the RIE etched diode separately to more clearly depict its *C-V* characteristics. With the exception of the B_0 diodes the C^{-2} vs V_R plots are essentially linear, as predicted by Eq. (19). They, however, have different slopes, and they intersect the voltage axis at distinctly different points. They have different slopes because the diodes have different concentrations of electron traps.

It must be noted that increasing C^{-2} with increasing reverse bias magnitude would be observed even in the absence of deep traps, due to the presence of the shallow *n*-type donors. The effective donor density N_{eff}, which is dependent upon the shallow donor density N_d, the trap density N_T, and the measurement angular frequency ω, may be given by[14]

$$N_{\mathrm{deff}} = N_d\left[1+\left(\frac{N_T}{n}\right)\frac{e_n^2}{e_n^2+\omega^2}\right]^2, \tag{24}$$

where n is the density of the free electrons in the bulk, and e_n is the emission rate of the traps. In order to extract the doping density of the $Al_xGa_{1-x}N$ layer, we carried out numerical calculations using Eqs. (19)–(23) and assuming $\varepsilon_s=9.4$. This value of the dielectric constant was estimated by using linear interpolation of the dielectric constants of GaN and AIN. It was noted that the use of the complex Eq. (24) for the effective doping did not bring significant change in the end result for the said frequency range, and that the capacitance per unit area of the diode was used in the respective equations for the calculation. The C^{-2} vs V_R relationships for A_0, B_0, C_0, and D_0 diodes are shown in Table III.

From the slopes of the C^{-2} vs V plot for the A_0 and C_0 diodes, the calculated doping density was 3×10^{16} $\mathrm{cm^{-3}}$. The slope of the same C^{-2} vs V plot for the sample D_0 diodes yielded the value of $N_d=1.6\times10^{16}$ $\mathrm{cm^{-3}}$, which is almost identical to that obtained from the Hall effect measurements. This confirms that there was considerable damage in the RIE etched only samples and in those those that were RIE etched and wet etched in aqua regia. It also confirms that the diodes, that had the RIE damage removed by a KOH etch, were essentially damage free.

The plots for the B_0 diodes, are problematic in that they were unstable for voltages >1 V, which might have been due to excessive leakage resulting from the plasma-induced damage. This is because there was an increase in the net doping concentration due to RIE etching. The increased tunneling current in the reverse bias for the B_0 diodes influenced

the measurements. For these diodes, there was a decrease in the slope of the C^{-2} vs V plot at low reverse voltage [see Fig. 6(b)], as there occurred a near-surface increase in the doping concentration. This is corroborated by reports from previous investigations.[26] It is very likely that there was a preferential loss of nitrogen due to plasma sputtering, which created nitrogen vacancies. These vacancies act as donor atoms. This is the probable cause of near-surface increase in doping density.

The flat-band (F-B) Schottky barrier heights for the present diodes were calculated using Eqs. (19)–(23). From the intercept of the C^{-2} vs V plot on the voltage axis, the contact potential was obtained as

$$V_{bi} = \frac{a_T}{b_T} + \frac{k_B T}{q}, \tag{25}$$

where a_T is the intercept of the C^{-2} vs V plot on the voltage axis. Using Eqs. (22) and (23) and assuming that the effective density of states in the conduction band of $Al_xGa_{1-x}N$ is $N_c = 2.8 \times 10^{18}$ cm^{-3}, we calculated F-B barrier heights for all the diodes except for the C_0 diode where V_{bi} was anomalously large for reasons that are not clear at this time. They are presented in Table I. The intercept used for the B_0 diodes is the one obtained at higher voltages [see Fig. 6(b)]. It can be seen that the F-B barrier height decreased from 0.55 eV for the A_0 diodes to 0.22 eV for the B_0 diodes. As indicated earlier, it is plausible that the plasma etching created a shallow damaged layer due to the preferential sputtering of nitrogen, thus enhancing the n-type coductivity. Creation of near-surface lattice defects, which generally behave as deep level states and thus can produce compensation, trapping or recombination in the material, are responsible for the enhanced tunneling. The latter caused a significant decrease in the F-B Schottky barrier height of the B_0 diodes. Due to rapid diffusion and ion channeling, these defects can be extended to as deep as 1000 Å. The decrease in the F-B barrier height for the RIE etched only samples is in line with the increase in reverse bias leakage current.

As it is evident from Table I, the boiling of a sample in KOH as a postetch treatment is very effective in removing the dry-etch damage and for improving the F-B Schottky barrier height. The Schottky barrier height for the D_0 diodes, as derive from C-V data, was 0.85 eV, which is closer to the theoretically calculated value for the $NiAl_xGa_{1-x}N$ diodes. As derived from reverse leakage current, this is, however, 0.57 V.

IV. CONCLUSION

In conclusion, Schottky contacts to n-$Al_xGa_{1-x}N$ have been fabricated on an untreated surface and surfaces treated by three different surface treatment techniques. Experiment is compared to theory to ascertain what the dominant effects of each treatment are. Samples that are RIE etched and then wet etched in a boiling KOH solution for 5 min produces the best electrical characterstics. The treatments are low damage Cl_2-based RIE etching of the sample prior to metal deposition, RIE etching of the sample and subsequent wet etching in boiling aqua regia for 5 min before metal deposition, and RIE etching of the sample and subsequent wet etching in boiling KOH for 5 min before metallization. The treatments appear to suppress the electrical activity of the dislocations in the diodes. Both current-voltage and capacitance-voltage measurements lead to this conclusion. This process demonstrates a significant improvement in the reverse leakage current density 3×10^{-3} A/cm^2 at 18 V; it also produces an ideality factor as low as 1.14, a reverse breakdown voltage over 44 V, and excellent forward conduction characteristics.

ACKNOWLEDGMENTS

The authors wish to thank Professor John Melngailis and Professor Jon H. Orloff for discussions, and for constructive comments on the paper. The research was carried out for partial fulfillment of the Ph.D. dissertation of Abhishek Motayed. It was supported by the NASA Goddard Space Flight Center, Greenbelt, Maryland Grant No. NAG5-11118 and the Army Research Laboratory Contract No. DAAD17-00-C-0092. The authors wish to thank Mr. Tony Gomez, Mr. James Griffin, and Mrs. Urmi Chatterjee for technical assistance.

[1]For a review of issues germane to *III-V* nitride materials and devices see, S. Noor Mohammad and Hadis Morkoç. J. Prog. Quantum Electron **20**, 361 (1996).
[2]S. Noor Mohammad, A. Salvador, and H. Morkoç, Proc. IEEE **83**, 1306 (1995).
[3]L. S. Yu, Q. Z. Liu, Q. J. Xing, D. J. Qiao, S. S. Lau, and J. M. Redwing, J. Appl. Phys. **84**, 2099 (1998). An interesting feature of the tunneling current component developed in this article is that it does not depend on the intrinsic carrier concentration which, for GaN and AlGaN, is very low.
[4]S. K. Noh and P. K. Bhattacharya, Appl. Phys. Lett. **78**, 3642 (2001); L. Wang, M. I. Nathan, T.-H. Lim, M. A. Khan, and Q. Chen, J. Appl. Phys. **68**, 1269 (1996).
[5]T. G. G. Maffeis, M. C. Simmonds, S. A. Clark, F. Peiro, P. Haines, and P. J. Parbrook, J. Appl. Phys. **92**, 3179 (2000); D. Qiao, L. S. Yu, S. S. Lau, J. M. Redwing, J. Y. Lin, and H. X. Jiang, *ibid.* **87**, 801 (2000); L. S. Yu, D. J. Qiao, Q. J. Xing, S. S. Lau, K. S. Boutros, and J. M. Redwing, Appl. Phys. Lett. **73**, 238 (1998); L. S. Yu, Q. J. Xing, D. Qiao, S. S. Lau, K. S. Boutros, and J. M. Redwing, *ibid.* **73**, 3917 (1998).
[6]E. D. Readinger, B. P. Luther, S. E. Mohney and E. L. Piner, J. Appl. Phys. **89**, 7983 (2001); U. Karrer, A. Dobner, O. Ambacher, and M. Stutzmann, Phys. Status Solidi A **176**, 163 (1999).
[7]A. Y. Polyakov, N. B. Smirnov, A. V. Govorkov, D. W. Greve, M. Skowronski, M. Shin, and J. M. Redwing, MRS Internet J. Nitride Semicond. Res. **3**, 37 (1998).
[8]L. Zhou, A. T. Ping, K. Boutros, J. Redwing, and I. Adesida, Electron. Lett. **35**, 745 (1999).
[9]A. P. Zhang *et al.*, Appl. Phys. Lett. **76**, 1767 (2000).
[10]A. P. Zhang *et al.*, Appl. Phys. Lett. **76**, 3816 (2000).
[11]T. Sawada, Y. Ito, N. Kimura, K. Imai, K. Suzuki, and S. Sakai, Appl. Surf. Sci. **190**, 326 (2002); S. Oyama, T. Hashizume, and H. Hasegawa, *ibid.* **190**, 322 (2002).
[12]K. Shiojima, J. M. Woodall, C. J. Eiting, P. A. Grudowski, and R. D. Dupuis, J. Vac. Sci. Technol. B **17**, 2030 (1999). Formation of small areas with low barrier height at the interface due to defects and dislocations is the key finding of this work. It also reports a significant difference in the F-B barrier height and Z-B barrier height for a contact with same doping in the semiconductor.
[13]S. Noor Mohammad, Z.-F. Fan, A. E. Botchkarev, W. Kim, O. Aktas, A. Salvador, and H. Morkoç, Electron. Lett. **32**, 598 (1996).
[14]K. Suzue, S. Noor Mohammad, Z.-F. Fan, W. Kim, O. Aktas, A. E. Botchkarev, and H. Morkoç, J. Appl. Phys. **80**, 4467 (1996).
[15]S. L. Rumyantsev *et al.*, J. Appl. Phys. **88**, 6729 (2000).
[16]M. Misra, A. V. Sampath, and T. D. Moustakas, Appl. Phys. Lett. **76**, 1045 (2000); see also, J. S. Foresi and T. D. Moustakas, *ibid.* **62**, 2859 (1993).
[17]J. Y. Duboz *et al.*, Appl. Phys. Lett. **69**, 1202 (1996).
[18]Yow-Jon Lin and Ching-Ting Lee, Appl. Phys. Lett. **77**, 3986 (2000); See

also, J.-K. Kim, J.-L. Lee, J.-W. Lee, Y. J. Park, and T. Kim, J. Vac. Sci. Technol. B **17**, 497 (1999).
[19]E. H. Rhoderick and R. H. Williams, *Metal-Semiconductor Contacts*, 2nd ed. (Clarendon, Oxford, 1988).
[20]S. M. Sze, C. R. Crowell, and D. Kahng, J. Appl. Phys. **35**, 2534 (1964).
[21]H. C. Card and E. H. Rhoderick, J. Phys. D **4**, 1589 (1971).
[22]R. F. Broom, Solid-State Electron. **14**, 1087 (1971).
[23]F. A. Padovani and R. Stratton, Solid-State Electron. **9**, 695 (1966).
[24]S. M. Sze, *Physics of Semiconductor Devices*, 2nd ed. (Wiley, New York, 1981), pp. 250–261.
[25]Abhishek Motayed, Muzar Jah, A. Sharma, W. T. Anderson, C. W. Litton, and S. Noor Mohammad, J. Vac. Sci. Technol. B **22**, 663 (2004); J.-L. Lee, J. K. Kim, J. W. Lee, Y. J. Park, and T. Kim, Solid-State Electron. **43**, 435 (1999).
[26]D. G. Kent *et al.*, Solid-State Electron. **45**, 1837 (2001).
[27]R. T. Tung, Phys. Rev. B **45**, 13509 (1992).
[28]S. Tiwari, *Compound Semiconductor Device Physics* (Academic, New York, 1992), Chap. 4.
[29]X. A. Cao, A. P. Zhang, G. T. Dang, F. Ren. S. J. Pearton, R. J. Shul, and L. Zhang, J. Vac. Sci. Technol. A **18**, 1144 (2000).
[30]A. P. Zhang *et al.*, J. Electrochem. Soc. **147**, 719 (2000).